buildings

MDPI

Article

Innovative Methods to Improve the Seismic Performance of Precast Segmental and Hybrid Bridge Columns under Cyclic Loading

Jahangir Badar [1], Tariq Umar [2,*], Muhammad Akbar [3], Nadeem Abbas [1], Qamar Shahzad [1], Weizhen Chen [1] and Muhammad Usman Arshid [4]

[1] School of Civil Engineering, Tongji University, Shanghai 200092, China
[2] Tariq Umar School of Architecture and Environment, University of the West of England, Bristol BS16 1QY, UK
[3] Institute of Mountain Hazards and Environment, Chinese Academy of Sciences, Chengdu 610000, China; akbarmohammad0092@gmail.com
[4] Department of Civil Engineering, University of Engineering and Technology, Taxila 47080, Pakistan
* Correspondence: tariq.umar@uwe.ac.uk

Abstract: This paper investigates the seismic performance of prefabricated segmental bridge columns (PSBCs) with hybrid post-tensioned tendons and energy dissipation (ED) bars under cyclic loading. PSBCs with unbonded and hybrid bonded prestressed tendons and columns incorporating ED bars are designed to improve the lateral strength, energy dissipation, and limit the residual drift. The PSBCs under cyclic loading were investigated using the three-dimensional finite element (FE) modeling platform ABAQUS. The FE model was calibrated against experimental results, with an overall error of less than 10%. The seismic performance of the proposed PSBCs was evaluated based on critical parameters, including lateral strength, residual plastic displacement, and the energy dissipation capacity. The results show that bonding the tendons in the plastic hinge region as opposed to the overall bonding along the column leads to a better cyclic performance. The lateral strength, and recentering abilities are further improved by bonding tendons up to 2/3 of the length in the plastic hinge region, along with 100–300 mm in the footing. It was also found that selecting a longitudinal length of ED bars crossing multiple precast segmental joints and having a circumferential spread of 70–90% of core concrete results in a higher bearing capacity and energy dissipation compared to ED bars crossing the single joint.

Keywords: prefabricated segmental bridge columns; seismic performance; numerical analysis; hybrid bonded tendons; ED bars; parameter analysis

Citation: Badar, J.; Umar, T.; Akbar, M.; Abbas, N.; Shahzad, Q.; Chen, W.; Arshid, M.U. Innovative Methods to Improve the Seismic Performance of Precast Segmental and Hybrid Bridge Columns under Cyclic Loading. *Buildings* **2024**, *14*, 1594. https://doi.org/10.3390/buildings14061594

Academic Editors: Constantin Chalioris, Alexandros-Dimitrios Tsonos and George Kalogeropoulos

Received: 27 March 2024
Revised: 10 May 2024
Accepted: 22 May 2024
Published: 31 May 2024

1. Introduction

Earthquakes have been a significant concern for bridge structures due to their complex and destructive nature [1]; the increasing rate of severe earthquakes has propelled engineers to look for alternative bridge designs and concepts to mitigate these concerns [2,3]. Prefabricated segmental bridge columns (PSBCs) have recently gained popularity. They have been a critical area of research for many scholars due to their resilient performance against earthquakes in low-to-medium seismic regions [3]. The resiliency of a structure is observed by how fast it can restore its functional responsibility without having to endure significant repairs after an earthquake. Compared with monolithic bridge columns, the major components of PSBCs are constructed in precast factories, which results in gaining several advantages such as a fast construction speed, less environmental impact, mitigating traffic jams, reduced noise pollution, and increased site safety [4,5].

PSBCs are stacked on top of each other. During an earthquake event, the piers segment rock back and forth. The energy is dissipated predominately by the joint's opening/closing mechanism instead of the formation of a plastic hinge, which is the crucial hysteric energy dissipation mechanism in monolithic columns. Hence, the inelastic deformations are mainly accommodated within the interface joints in the segments, and the column retains its recentering ability for higher drift levels [6].

Several researchers have studied the potential use of rocking systems as a passive mitigation technique for structures undergoing earthquake loading and have identified that these systems are beneficial in reducing damage and residual deformations. However, the outcome is a reduction in energy dissipation, hence limiting the damping capabilities of the structure [7], which results in a deficient seismic performance; therefore, the application of PSBCs in medium–strong seismic regions has been limited. Various methods to improve the seismic performance of PSBCs have been reported in the literature. The usage of innovative structural configurations and high-performance materials [8–11], fiber-reinforced polymers (FRPs) [9,10,12], or circular steel tubes [13–15], hybrid columns with cast in place (CIP) concrete at the hinge area [16–18], elastomeric pads [19], steel shear resistant connectors [20], and hybrid steel bars [21] increases the energy dissipation capacities of prefabricated columns and retains the self-centering capabilities. These systems have been beneficial, but they contribute to the complexity of the design and incur additional fabrication costs.

The critical component of the precast segmental bridge piers is the post-tensioned tendons. The segments of these piers are held together by providing a clamping force through post-tensioned tendons, which keep the sections intact and offer essential resetting abilities to the system. As reported in previous studies, both unbonded and bonded post-tensioned tendon systems are used in practice. The unbonded tendon systems result in minimal residual deformation, reduced energy dissipation, and a higher ductile capacity [22,23]. In contrast, the bonded tendon system results in more significant residual drifts, improved lateral strength, and energy dissipation, primarily due to the strong bond between the grout and tendons along with induced cracks and damage to concrete around the strands [24–26]. Researcher Wang and his team proposed the concept of the hybrid-bonded system in which bonded tendons were used at the edge of the section [27,28]. In contrast, unbonded ones were used in the middle section. This type of bonded system was compared with bonded–unbonded systems, and it was observed that hybrid-bonding systems could provide a more ductile capacity, lesser residual displacement, and an improved energy dissipation capacity.

These studies have been beneficial in understanding the bonding conditions of the prestressing system. Still, there is a lack of studies on the quantitative impact of hybrid bonding on the seismic performance of PSBCs. Detailed suggestions regarding their usage in different seismic regions and the influence of various design parameters of this novel hybrid bonding technique are missing.

Another vital parameter to improve the seismic performance of PSBCs has been the usage of mild steel bars crossing the joints of the precast segments, commonly known as energy dissipation bars (ED bars). These bars have been used in different structural configurations such as exterior energy dissipaters [29–31], interior energy dissipation bars [32–35], and high-strength steel rebars as energy dissipaters [36], with different shapes of piers such as circular [34] and rectangular [37]. The researcher Li and his team investigated the energy dissipation capacities of circular segmental bridge columns based on the experimental models of Hewes and Priestley, and found that increasing the ratio of internal mild steel bars increases the energy dissipation with a rise in the residual drift [14,38]. Later on, Wang et al. 2018 conducted extensive work on the usage of ED bars in ultra-high-performance concrete (UHPC) hollow rectangular specimens, focusing on the equivalent and additional unbounded lengths of ED bars [39]. The research was based on the concept of an equivalent plastic hinge model. These studies found that using ED bars increases the overall energy dissipation of the system. The contribution of ED bars to the

total lateral strength of no more than 25% is suitable. Increasing the post-tensioning levels up to 44% of yield strength instead of increasing the PT ratios leads to a significant improvement in the seismic performance of PSBC systems incorporating energy dissipaters.

While considerable research has been done to evaluate and improve the energy dissipation capacities of PSBC by using different types of dissipaters. However, there is still a lack of knowledge about the impact of various configurations of internal ED bars on the seismic performance of circular PSBCs.

This paper focuses on collectively improving three critical parameters (the bearing capacity, energy dissipation, and residual drift) to obtain a better-performing PSBC system. Two PSBC systems are utilized: (1) PSBC with hybrid-bonded tendons and (2) PSBC with unbonded tendons and ED bars. The cyclic loading performance of these systems is compared with PSBC, which incorporates unbonded tendons to study their efficiency. A three-dimensional (3D) finite element (FE) model based on the experiment conducted by Zhang et al., 2019 under the application of cyclic loads is accurately validated [11]. A new type of hybrid bonding focusing on systematic bonding across the plastic hinge region, non-plastic hinge region, and through the critical joint (the joint between the footing and bottom segment) is proposed. A comprehensive parametric analysis is carried out, including the influence of hybrid bonding conditions, the influence of the lengths of ED bars, and the influence of the arrangement of ED bars. The essence remained upon finding a balanced system with improved hysteric characteristics, ductile deformation, and energy dissipation capacities. The impact of seismic performance indicators such as ductility, energy dissipation, and residual plastic deformation is expected to provide engineering design references.

2. Limit-State Capacities

In this paper, the limit-state capacities are based upon the design concept of China's seismic design of building structures in combination with the detailed specifications for the seismic design of highway bridges (JTG/T B02-01-2008) [MOT, 2008] [40,41]. According to these specifications, the structures are designed so small-scale earthquakes do not harm their structural integrity, medium-scale earthquakes can be repaired, while large-scale earthquakes should not fail. During ground motion excitation, joint opening in the base segment of the PSBCs occurs due to the rocking mechanism. Concrete's longitudinal and transverse reinforcements express the primary damage. The concrete at the compressive edge shows yielding, spalling, and crushing. The primary longitudinal reinforcements (post-tensioned tendons) show elastic and yield states, while the transverse and longitudinal reinforcements will show yielding, hardening, and fracturing. Due to the self-centering capacities of PSBC's, the residual plastic deformation is also used as an evaluation parameter.

The limit-state capacity can be defined as the capability of the bridge components to endure an earthquake event without exceeding the pre-defined performance level [42]. These limits describe the entrance of bridge components into prescribed damage states [43]. The PSBCs used in this research are divided into two levels according to their potential damage characteristics, as shown in Table 1. Among them, performance targets 1 and 2 correspond to small and large earthquake events. The parameters used to analyze the limit-state capacities are the compressive strain of concrete, the tensile stress of reinforcement, the prestress levels of tendons, and the residual plastic deformation. In Table 1, the prestress level refers to the relationship between the tensile force of prestressed tendons and the yield strength of steel strand materials. The residual deformation of the pier column refers to the ratio of the pier top's residual displacement to the pier column's effective height when the horizontal load is unloaded to 0. Here, the residual deformation limit is 1% calibrated in the Japanese Code JRA, 2002 [44].

Table 1. Limit-states for proposed PSBC's.

Performance Target	Function	Concrete Strain	Reinforcement Strain	Prestress Level (%)	Residual Drift (%)
Target 1	Normal use	−0.004	0.015	-	-
Target 2	Hidden danger	−0.018	0.1	80	1%

3. Hybrid Post-Tensioned Tendons Concept

The role of post-tensioned tendons is pivotal in PSBCs. Unbonded tendons contribute to enhancing lateral strength, ductility, and facilitating recentering abilities [45]. However, bonded tendon systems have been explored to address the limitations of unbonded tendons in terms of energy dissipation [34]. While bonded systems initially boost lateral strength and overall energy dissipation, they suffer from a reduced ductile capacity due to premature tendon yielding, leading to a diminished axial force, shear resistance, and strength degradation. Previous studies have underscored that the premature failure of bonded post-tensioned tendons in PSBCs is attributed to the selection of higher axial stresses and initial prestressing forces [34,46]. Other researchers have demonstrated that selecting an axial compression ratio of less than 20% and initial prestressing forces of 25–30% of the yield stress resulted in improved lateral strength and energy dissipation [26–28]. However, this approach still led to higher residual displacements, restricting its application to low seismic regions. The concept of a hybrid post-tensioned system aims to enhance lateral strength and energy dissipation, and control residual displacements, making hybrid PSBCs suitable for medium–high seismic regions. A performance assessment will adhere to detailed limit state capacities discussed previously.

The application of hybrid bonded tendons involves a modification of the traditional bonded system. In the traditional approach, the tendon is encased in a corrugated tube, and cementitious materials are injected after applying a prestressing force. In the hybrid approach, bonded–unbonded properties are integrated into each tendon of PSBCs using a similar method. However, the cementitious material is applied only to specific regions of the tendon, while other sections remain unbonded. This is achieved by covering designated areas of the tendon with PVC pipes or duct tape, preventing contact with the surrounding concrete, and maintaining an unbonded status, as depicted in Figure 1.

Comparatively, the hybrid-bonded system offers several advantages over traditional systems. By selectively bonding tendons, a greater lateral strength and increased energy dissipation are anticipated compared to PSBCs with fully unbonded tendon systems. Meanwhile, maintaining unbonded sections ensures recentering abilities and improved ductile capacities, even at higher drift levels, due to the fact that the whole lengths of the tendons will not deteriorate with the surrounding concrete, resulting in them surpassing the performance of traditional bonded tendon configurations.

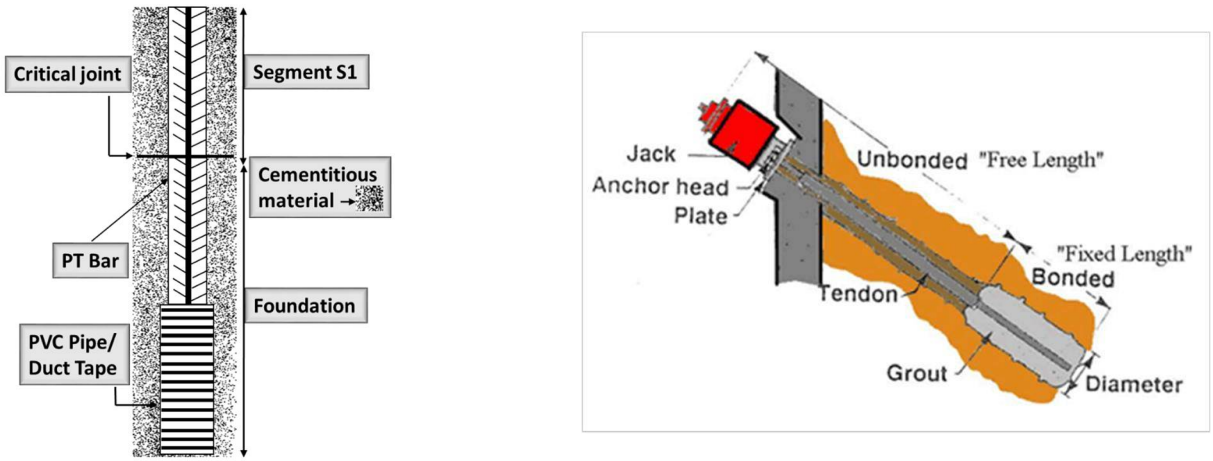

Figure 1. Hybrid-bonding concept in PSBC.

4. Numerical Modeling

A detailed description of 3D FE models with modeling methods and procedures is presented, and the models are developed using ABAQUS 6.13. (2013) [47]. The accuracy of the numerical model is demonstrated by calibrating with experimental results; later on, the models are used for an extensive parametric analysis.

The specimen was designed with four prefabricated segments, each having a height of 400 mm and a 350 mm diameter. The total height of the specimen was 1800 mm (denoted by the distance from the column base to the mid-point of the loading block), as shown in Figure 2. All the segments were constructed with regular concrete, having a measured concrete strength of 47.0 MPA.

Transverse spirals confined the upper segments to a diameter of 6 mm with a 50 mm center-to-center spacing, while the bottom segments had a spacing of 80 mm. The longitudinal reinforcements were used to hold and position spiral reinforcements. Three unbounded prestressed tendons were used to connect the loading block, segments, and footing with each other. The material properties of concrete, longitudinal reinforcements, transverse reinforcements, and prestressed tendons are given in Table 2, whereas Figure 2 shows the cross-sectional details of PSBC-1.

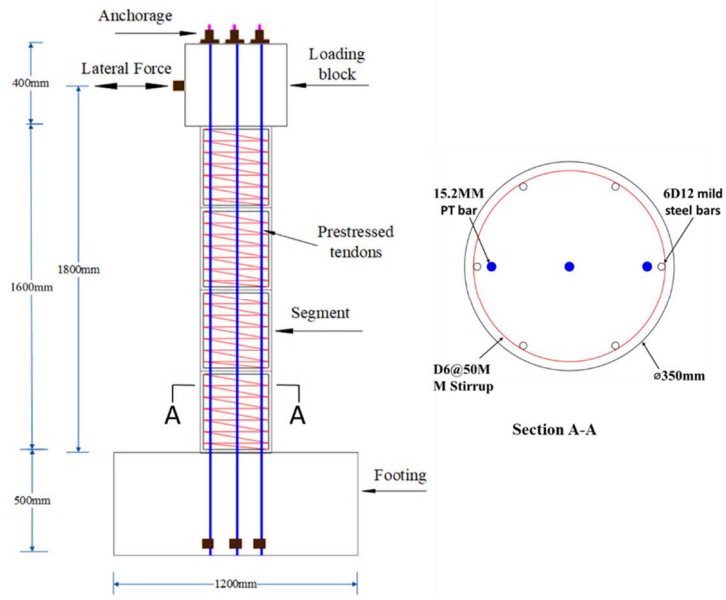

Figure 2. Cross-sectional and reinforcement details of PSBC-1.

Table 2. PSBC material properties.

Component	Property	Value
Concrete	Strength (MPA)	47.0
	Poisson's ratio	0.2
	Elastic modulus (GPA)	34.5
Transverse reinforcements	Yield stress (MPA)	335.0
	Poisson's ratio	0.3
	Elastic modulus (GPA)	210
Longitudinal reinforcements	Yield stress (MPA)	335.0
	Poisson's ratio	0.3
	Elastic Modulus (GPA)	200
Prestressed Tendons	Yield stress (MPA)	1670
	Ultimate Stress (MPA)	1860
	Poisson's ratio	0.3
	Elastic Modulus (GPA)	195

All the components made up of concrete, including the column segments, footing, and beam, and were modeled with eight-node 3D brick elements (C3D8R), which helps avoid the hourglass phenomenon caused by large deformation. The concrete damage plasticity model (CDP) is explicitly designed for reinforced concrete structures subjected to monotonic and dynamic loadings, and its performance in capturing the overall behavior of concrete is impeccable [48]. The CDP model has a higher rate of convergence when compared with other plasticity models because the column studied in this manuscript is a reinforced concrete column subjected to cyclic loadings. Therefore, the CDP model is adopted to simulate the inelastic behavior of the column mentioned above.

The Abaqus/standard CDP model uses the models proposed by scholars Lubliner and Lee [49,50], which include an elastic modulus, poison's ratio, and five plasticity parameters, as shown in Table 3, to define the yield surface function, potential flow, and viscosity of the material. The stress–strain relationship of concrete developed by Mander [13] was used in this study. The compressive and tensile behaviors of concrete are described by two sets of uniaxial data along with damage data, which decreases the material's stiffness under repeated loading. These data are input into the system using a tabulated form of yield stress versus inelastic strain and yield stress versus cracking strain, respectively [47].

Table 3. CDP plasticity parameter in ABAQUS.

Parameter	Value	Explanation [SIMULIA, 2012] [47]
ψ	38	Dilation angle
e	0.1	Flow potential eccentricity
σ_{bo}/σ_{co}	1.16	The ratio of initial equibiaxial yield stress to uniaxial compressive yield stress
K_c	0.6666667	The coefficient determining the shape of the deviatoric cross-section
μ	0.00001	Viscosity parameter

The steel reinforcements, including longitudinal and spiral reinforcements, were modeled with Truss elements (T3D2) and were embedded in the surrounding concrete by applying embedded region constraints with a steel cage as an embedded region and the whole model as a host region in order to simulate concrete core confinement [47] accurately.

Three D15.22 mm unbonded tendons were modeled with beam elements (B31) with small portions of tendons embedded in a footing and loading block to model tendon anchorage, as shown in Figure 3. For the parametric studies of hybrid-bonded tendons, the sections injected with the cementitious material were embedded within the surrounding sections of concrete to simulate the hybrid-bonded tendon system, following the bonded–unbonded tendon simulation technique described in the literature [38]. The elastic–perfectly plastic model was utilized to simulate the stress–strain constitutive relationship for the steel reinforcements and prestressed tendons [51].

The tendons were designed to remain elastic during the application of cyclic loadings. Therefore, the initial prestressing levels (fps/Fyt, where fps is the prestressing stress and Fyt is the yield strength of the tendon) of 25% (PT L&R) and 30% (PT-MID) were selected, which helped to preserve the axial force and recentering abilities of the column [33,34].

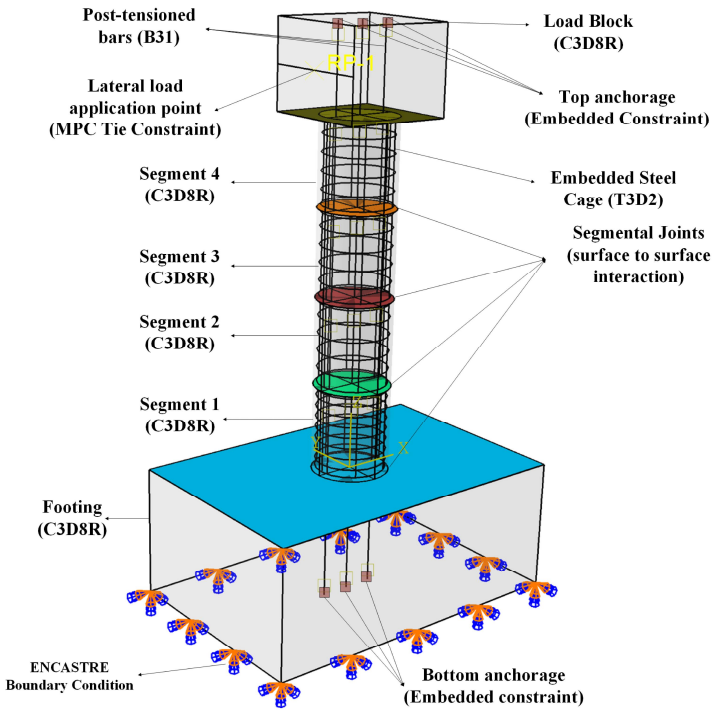

Figure 3. Model details of PSBC-1.

The prestressing effect is modeled through either the (1) initial strain or (2) initial temperature load. This study used the pre-defined field temperature to simulate the initial stress of the prestressed tendons.

During the tests, the footing was fixed to the stable floor using two high-strength rods placed through the footing and anchored into the floor. The ENCASTRE boundary condition, having translational (Ux = Uy = Uz = 0) and rotational (UR1 = UR2 = UR3 = 0) degrees of freedom for all the nodes of the bottom surface, was utilized to simulate the fixed boundary conditions, as shown in Figure 3. The rocking columns experience joint opening/closing behavior under lateral cyclic loadings. In order to simulate this behavior, the surface-to-surface contact elements were defined. The interaction between the concrete surfaces was modeled by normal contact, with default constraint enforcement and hard contact pressure over-closure having finite sliding. The tangential contact behavior between the master and slave surface was modeled by tangential friction; the tangential friction was assumed to be 0.5, as proposed by Dawood [52], between the segments. The surfaces developed compression when in contact with each other and were allowed to separate without resistance.

The loading was applied in two stages. During the first stage, a prestressing force was applied by using pre-defined field temperatures. During the second stage, lateral displacement-controlled cyclic loadings were imposed on the reference point of the loading block with pre-defined drift values. MPC constraints with tie connections were used for the reference point, and loadings in the models were the same as those conducted in the tests [47]. The loading cycle was conducted as the displacement control, and the drift levels included 0.1%, 0.2%, 0.3%, 0.5%, 0.75%, 1%, 1.5%, 2%, 2.5%, 3%, 3.5%, 4%, 4.5%, 5%, 6%, 7%, and 8%. Each drift was applied for two cycles; the model details are shown in Figure 4.

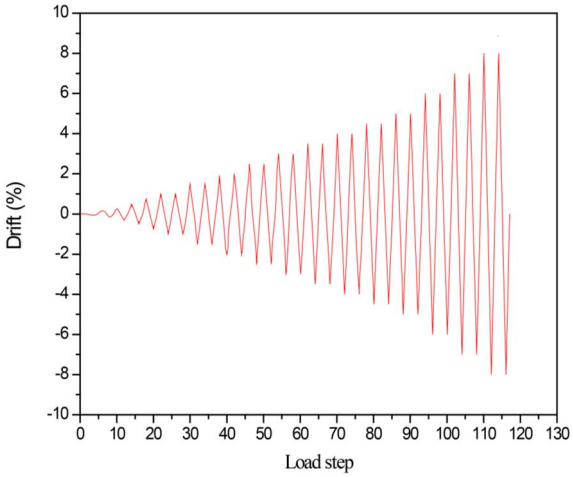

Figure 4. Repeated cyclic loading history.

5. Model Validation and Analysis

To accurately verify the proposed numerical model, the results are validated against the experiment [11]. In this study, the numerical models are calibrated against the experimental results in terms of force–displacement hysteric curves, as shown in Table 4 and Figure 5. The numerical model was able to capture the force–displacement response quite accurately in both the loading and unloading directions, with an overall error of less than 10%. The simulation results can effectively predict the horizontal bearing capacity, residual displacement, and ductility of PSBCs. The hysteric response at higher drifts is more complicated than at lower drifts; the numerical models usually have difficulty in accurately predicting the response at higher drifts. This study obtained excellent calibration, indicating that crucial features of PSBCs, such as concrete material models, reinforcement models, joint opening/closing mechanisms, and post-tensioning tendons, were modeled correctly. The simulation technique for bonding the tendons is well-established in the literature [38]. It involves embedding the bonded length of tendons within the surrounding concrete to simulate anchorage for unbonded tendons and full embedment for bonded ones. Model validation using the anchorage bonded technique demonstrated excellent calibration. Therefore, both the findings of this research and evidence from the literature are considered to validate the results of hybrid-bonded tendons in parametric simulations. Figure 6 shows the comparison of the compressive strain of the cover concrete. From the vertical strain distribution of the bottom section of the specimen, it can be seen that the compressive strain of concrete is concentrated at the bottom joint (the joint between the foundation and bottom segment). After selecting a node at the maximum strain position at the joint, the maximum compressive strain of the concrete reached a level of −0.004 for the first time when the displacement amplitude approached 1.73%. According to the performance target limits mentioned in Table 1, this threshold can be used as the calibration of performance target 1, which indicates that at a 1.73% displacement amplitude, the concrete cover at the joint position will peel off and be crushed.

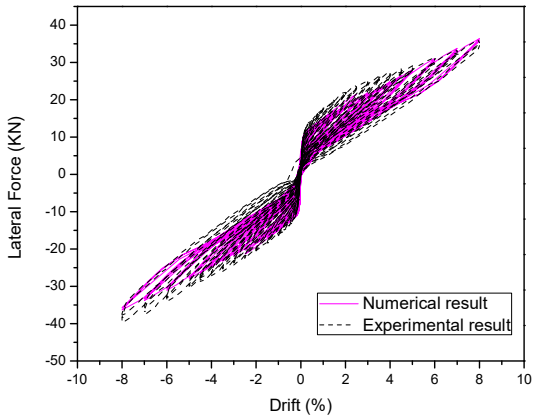

Figure 5. Lateral force results of experiment and numerical model.

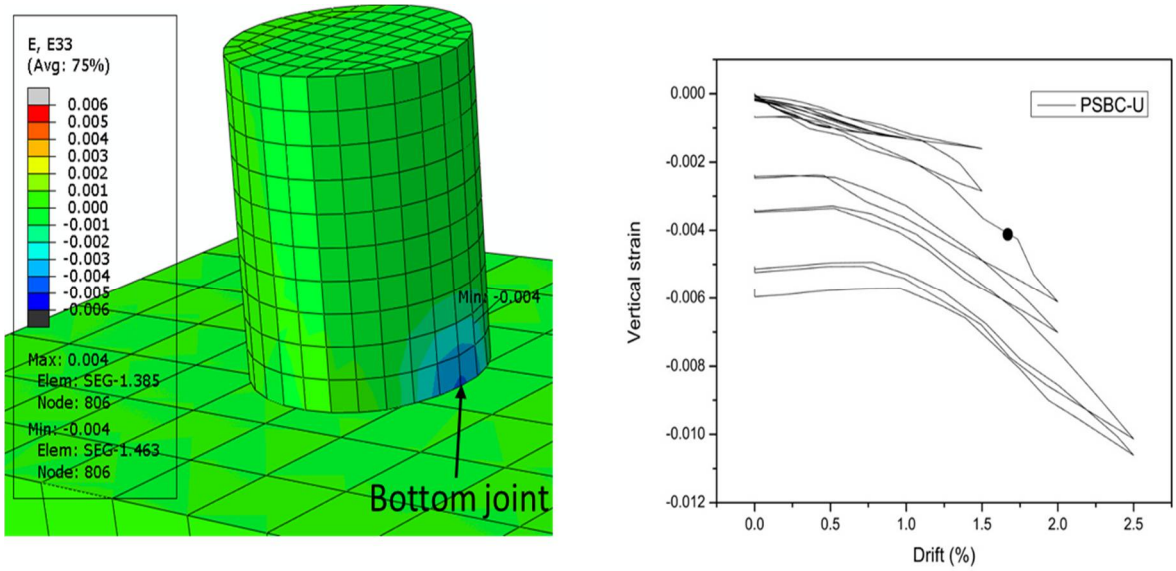

Figure 6. Maximum compressive strain of cover concrete.

Table 4. Lateral forces and errors and different drift ratios.

Drift Ratio (%)	Experiment (KN)	Numerical (KN)	Error (%)
0.1	9.81	9.88	0.71
−0.1	−9.45	−9.97	5.5
0.5	13.6	12.74	6.32
−0.5	−13.5	−12.75	5.55
1	17.69	16.01	9.49
−1	−15.94	−14.94	6.27
3	23.96	21.61	9.8
−3	−22.96	−21.23	7.53
5	28.12	27.65	1.67
−5	−29.26	−27.6	5.67
7	32.16	33.36	3.73
−7	−35.02	−33.28	4.96
8	35.93	35.91	0.05
−8	38.53	−35.83	7

The comparison of the maximum edge compressive strains of core concrete is shown in Figure 7; it can be seen that the compressive strain of confined concrete is also concentrated at the bottom joint. The tensile strain occurs in concrete fiber near the edges of the section. The concrete unit connected with the bottom joint, as shown in Figure 7, is selected for analysis. When the displacement amplitude reached 6%, the compressive strain reached −0.018 for the first time. This level can be used to calibrate performance target two for the specimen. It must be noted that neither the strain of transverse reinforcement nor the residual plastic displacement reached the prescribed levels mentioned in Table 1 earlier than the compressive strain of concrete in order to be considered for the calibration of performance targets.

Additionally, the prestressed tendons never showed a yield state. In this paper, performance target one refers to the yield state of the pier, and performance target two describes the limit state beyond which the performance of piers under the earthquake ground motions has a hidden danger of use. Hence, the displacement ductility index is defined as the ratio of the limit state to the yield state. The displacement ductility ratio was calibrated with an error in the calculation of 10%. The difference in the calculation in this study is acceptable when considering that the non-linear numerical model has various uncertainties.

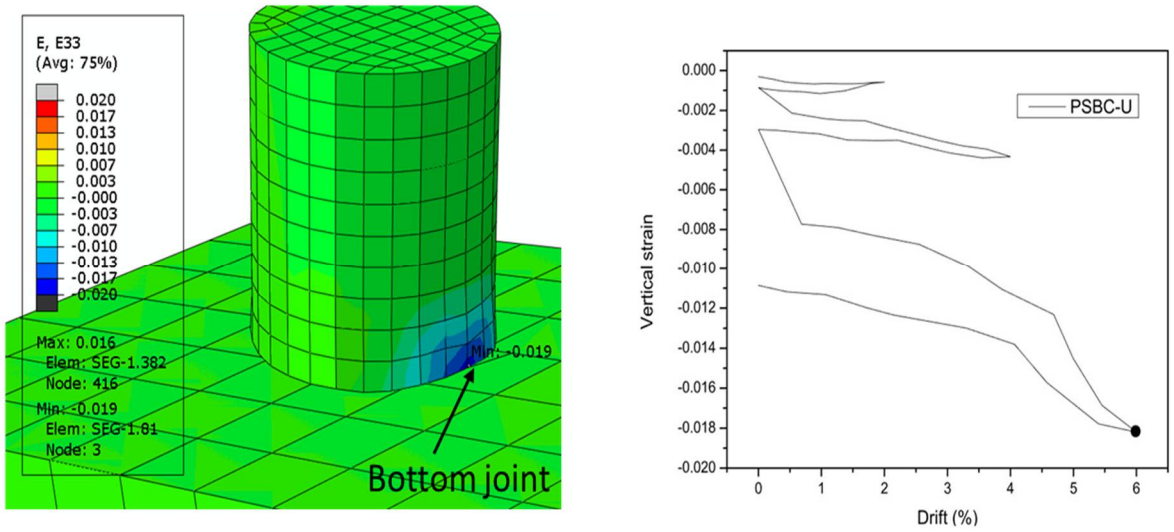

Figure 7. Maximum compressive strain of core concrete.

6. Parameter Study

After verifying the specimen, the model was used as the reference column to perform detailed parametric studies without losing the generality. As described in Table 5, the influence of different parameters is investigated. The design parameters are adjusted using the same numerical model for a valid comparison.

Table 5. Different design parameters of specimens.

Specimen	Axial Ratio	Bonding Condition	Bonded Length in PH	Bonded Length in Non-PH	Bonded Length in Footing	ED Bars	ED Bars Length above Footing	Ed Bars Spread (%) of Core Concrete
PSBC-U	0.1	Unbonded	-	-	-	-	-	-
PSBC-1	0.1	Hybrid-bonded	100 mm	-	-	-	-	-
PSBC-2	0.1	Hybrid-bonded	200 mm	-	-	-	-	-
PSBC-3	0.1	Hybrid-bonded	300 mm	-	-	-	-	-
PSBC-4	0.1	Hybrid-bonded	400 mm	-	-	-	-	-

PSBC-5	0.1	Hybrid-bonded	-	100 mm	-	-	-	-
PSBC-6	0.1	Hybrid-bonded	-	200 mm	-	-	-	-
PSBC-7	0.1	Hybrid-bonded	-	400 mm	-	-	-	-
PSBC-8	0.1	Hybrid-bonded	200 mm	-	100 mm	-	-	-
PSBC-9	0.1	Hybrid-bonded	300 mm	-	100 mm	-	-	-
PSBC-10	0.1	Hybrid-bonded	200 mm	-	300 mm	-	-	-
PSBC-11	0.1	Hybrid-bonded	300 mm	-	300 mm	-	-	-
PSBC-12	0.1	Hybrid-bonded	400 mm	-	300 mm	-	-	-
PSBC-E1	0.1	Unbonded	-	-	-	6D12 mm	200 mm	-
PSBC-E2	0.1	Unbonded	-	-	-	6D12 mm	400 mm	-
PSBC-E3	0.1	Unbonded	-	-	-	6D12 mm	600 mm	-
PSBC-E4	0.1	Unbonded	-	-	-	6D12 mm	800 mm	-
PSBC-S90L1	0.1	Unbonded	-	-	-	6D12 mm	200 mm	90
PSBC-S70L1	0.1	Unbonded	-	-	-	6D12 mm	200 mm	70
PSBC-S50L1	0.1	Unbonded	-	-	-	6D12 mm	200 mm	50
PSBC-S30L1	0.1	Unbonded	-	-	-	6D12 mm	200 mm	30
PSBC-S90L2	0.1	Unbonded	-	-	-	6D12 mm	400 mm	90
PSBC-S70L2	0.1	Unbonded	-	-	-	6D12 mm	400 mm	70
PSBC-S50L2	0.1	Unbonded	-	-	-	6D12 mm	400 mm	50
PSBC-S30L2	0.1	Unbonded	-	-	-	6D12 mm	400 mm	30
PSBC-S90L3	0.1	Unbonded	-	-	-	6D12 mm	600 mm	90
PSBC-S70L3	0.1	Unbonded	-	-	-	6D12 mm	600 mm	70
PSBC-S50L3	0.1	Unbonded	-	-	-	6D12 mm	600 mm	50
PSBC-S30L3	0.1	Unbonded	-	-	-	6D12 mm	600 mm	30
PSBC-S90L4	0.1	Unbonded	-	-	-	6D12 mm	800 mm	90
PSBC-S70L4	0.1	Unbonded	-	-	-	6D12 mm	800 mm	70
PSBC-S50L4	0.1	Unbonded	-	-	-	6D12 mm	800 mm	50
PSBC-S30L4	0.1	Unbonded	-	-	-	6D12 mm	800 mm	30

6.1. Influence of Bonding Conditions

6.1.1. Hybrid Bonding in the Plastic Hinge Region

The bonded and unbounded post-tensioned tendons are commonly used to clamp the precast segments, as reviewed previously. The unbounded tendons are beneficial for their more exceptional recentering abilities and minimal residual displacements, with lower energy dissipation as their detrimental aspect. In contrast, the bonded tendons have a higher ultimate lateral strength, energy dissipation, and more considerable residual drift, resulting in columns being unfit for repair and retrofitting.

This paper proposes a novel hybrid bonding condition, which systematically incorporates the bonded and unbonded properties together in every tendon to improve the horizontal bearing capacity energy dissipation while reducing the residual drift, to ensure that the columns can maintain their performance criteria in case of high lateral drifts and can easily be retrofitted and reused after a major earthquake, PVC pipes can be used to cover the proposed sections of tendons, which will be unbonded. As a result, when the cementitious materials are inserted into the grouts, the sections covered by PVC pipes will not come into contact with the surrounding concrete and, hence, remain unbonded. The tendons were bonded as a percentage of the plastic hinge region (the potential plastic hinge region is defined as the greater of the column diameter and 1/6th of the distance from the column base to the loading point) such as 25%, 50%, 75%, and 100% of the length of the plastic hinge region, denoted as PSBC-B1, PSBC-B2, PSBC-B3, and PSBC-B4. The specimen's hysteric curves are superimposed on each other and compared with PSBC (with unbonded tendons), denoted as PSBC-U, as shown in Figure 8a, with the cumulative energy dissipation shown in Figure 8b, and residual displacement in Figure 8c.

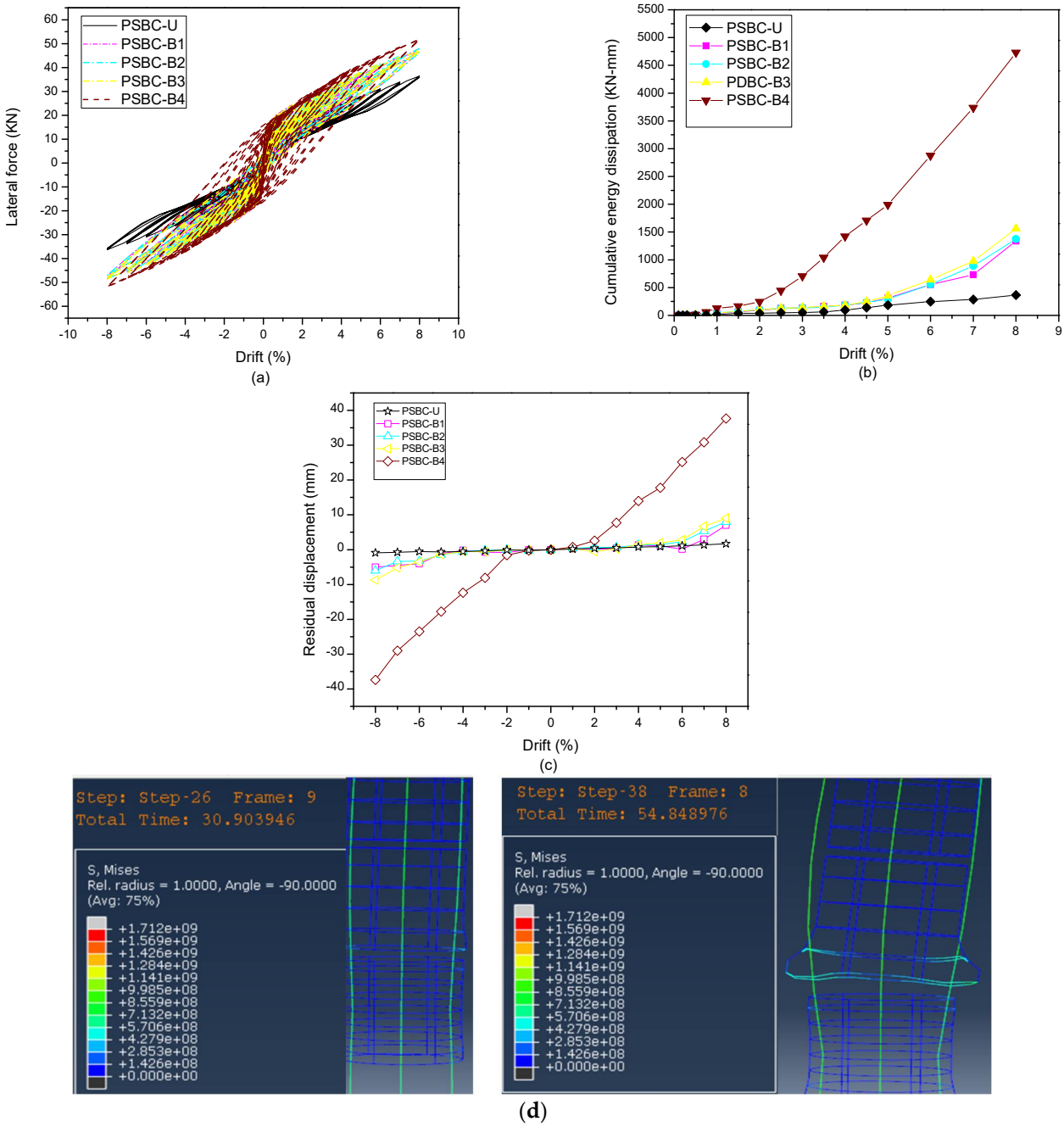

Figure 8. Comparison of hybrid-bonded and unbonded PSBCs in hinge area (**a**) hysteric force, (**b**) cumulative energy dissipation, and (**c**) residual displacement. (**d**) Stress concentration in the segment 3–4 joint area due to selection of 400 mm bonded length.

In the rocking mechanism system, the main joint is the segment4-foundation joint, with the plastic hinge region located above that joint. When the tendons are bonded within this area, energy is dissipated by the joint opening–closing mechanism, along with the deformation of surrounding concrete in the bonded tendon regions. Optimal performance occurs when the tendons are bonded within 100–300 mm of the plastic hinge region, preventing premature failures. However, selecting a bonded length of 400 mm, which extends beyond the plastic hinge to the joint between segments 3–4, leads to a greater stress concentration within this area, as shown in Figure 8d. Additionally, the lack of joint opening–closing within this segment prevents energy dissipation, resulting in excessive concrete damage and transverse reinforcement failure, leading to the loss of structural integrity and higher residual displacement. Hence, balance is achieved by bonding

the tendons in the plastic hinge region, where the influence of the segment4-foundation joint is predominant. Here, the joint-opening and closing mechanism can help dissipate some energy to preserve structural integrity while allowing hybrid-bonded tendons to play a positive role instead of the negative role they play in the segments 3–4 joint, respectively.

Using bonded tendons completely across the plastic hinge region resulted in increased ultimate lateral strength and energy dissipation compared to PSBC-U. The maximum lateral strength of PSBC-B4 was 51.85 kN, which is 30.74% greater than PSBC-U; energy dissipation was greatly enhanced, but with a substantial increase in residual displacement (37.65 mm), which equals to a 2.09% drift level. The ultimate lateral strength signifies the peak resistance a structure offers against lateral forces. Energy dissipation involves the conversion of mechanical energy into other forms, thus diminishing the transmitted forces and mitigating damage, typically quantified by the area under the hysteric curve. Residual displacement in PSBCs denotes the lingering movement or deformation post-seismic loading, computed by subtracting initial displacement from final displacements following cyclic loading cessation. PSBC-B1, PSBC-B2, and PSBC-B3 also showed increasing patterns of ultimate lateral strength energy dissipation compared to PSBC-U, but with much reduced residual displacement compared to PSBC-B4. According to the limit-state capacity analysis, it is observed that increasing the length of hybrid bonding in the plastic hinge region improves both the initial elastic stiffness and the horizontal yield-bearing capacity of piers. The initial elastic stiffness represents structural stiffness or rigidity during the initial phase of loading which is measured in terms of the force required to produce a certain displacement in the structure. Meanwhile, the horizontal yield-bearing capacity indicates the maximum drift or displacement that the structure can sustain before reaching the yield point, as outlined in the limit state capacity section. The displacement capacity and ductility of piers decrease with the increased bonded length, mainly because the increased bonding length of tendons results in increased damage in the concrete surrounding the bonded regions. The displacement capacity and ductility can be defined as the maximum drift sustained by the column without a significant reduction in the load-carrying capacity, as mentioned in performance criteria two of the limit state capacities. The lateral bearing strength values are recorded corresponding to this limit. The values above this threshold will have hidden dangers.

Additionally, the limit-state bearing capacity increases with an increase in the bonded length, as shown in Table 6; for low seismic regions, bonding tendons completely across the plastic hinge region will be a better option than partial bonding due to the higher yield and limit-state lateral strength, along with improved energy dissipation provided by PSBC-B4. Also, the risk of losing the recentering ability will be lower due to the not-so-drastic increase in the residual plastic displacement, as evident in Figure 8c, at lower drift levels. In contrast, the ultimate lateral strength and energy dissipation contributions are significant at higher drift levels. However, since the ductility and displacement capacity decrease, a significant increase in the residual plastic deformation beyond the safety limits described in Table 6 may lead to unrepairable conditions. Therefore, using partial bonding across the plastic hinge regions, as shown in PSBC-(1-3), will be a better option in medium–high seismic regions.

Table 6. Response parameters of specimens bonded in the plastic hinge region.

Specimen	Yield State		Limit State		Displacement Ductility Ratio
	Force (KN)	Drift (%)	Force (KN)	Drift (%)	
PSBC-U	17.08	1.73	30.61	6	3.46
PSBC-B1	23.34	1.37	36.83	5	3.64
PSBC-B2	23.83	1.5	37.72	5	3.33
PSBC-B3	24.45	1.6	38.6	4.5	2.81

PSBC-B4	29.52	2.5	39.01	4	1.6

This novel approach outperforms existing solutions, such as bonded and unbonded tendons, in terms of lateral strength, energy dissipation, and residual displacement. Bonded tendons often lack sufficient lateral strength and energy dissipation, while unbonded tendons result in high residual displacement. Additionally, compared to other optimization strategies for PSBC designs, such as steel-jacketing and the use of costly materials like high-strength bars and fiber polymers, this concept offers a promising, cost-effective, and straightforward design alternative.

6.1.2. Hybrid Bonding across Non-Plastic Hinge Region

To quantitatively and qualitatively analyze the effects of hybrid bonding in non-plastic hinge regions, segment S-4 (which is the uppermost segment) was chosen to model the specimens. PSBC-B5, PSBC-B6, and PSBC-B7 with a 25%, 50%, and 100% length bonded across segment S-4 were selected for analysis. The results of the lateral force, energy dissipation, and response parameters are shown in Figure 9a,b, and Table 7.

Table 7. Response parameters of specimens bonded in the non-plastic hinge region.

Specimen	Yield State		Limit State		Displacement Ductility Ratio	Residual Displacement (mm)
	Force (KN)	Drift (%)	Force (KN)	Drift (%)		
PSBC-U	17.08	1.73	30.61	6	3.46	1.7, −0.89
PSBC-B5	21.67	1.5	35.79	5.4	3.6	4.3, −3.8
PSBC-B6	22.25	1.4	33.27	4.5	3.18	5.2, −2.84
PSBC-B7	21.63	1.5	31.57	4	2.66	8.5, −5.2

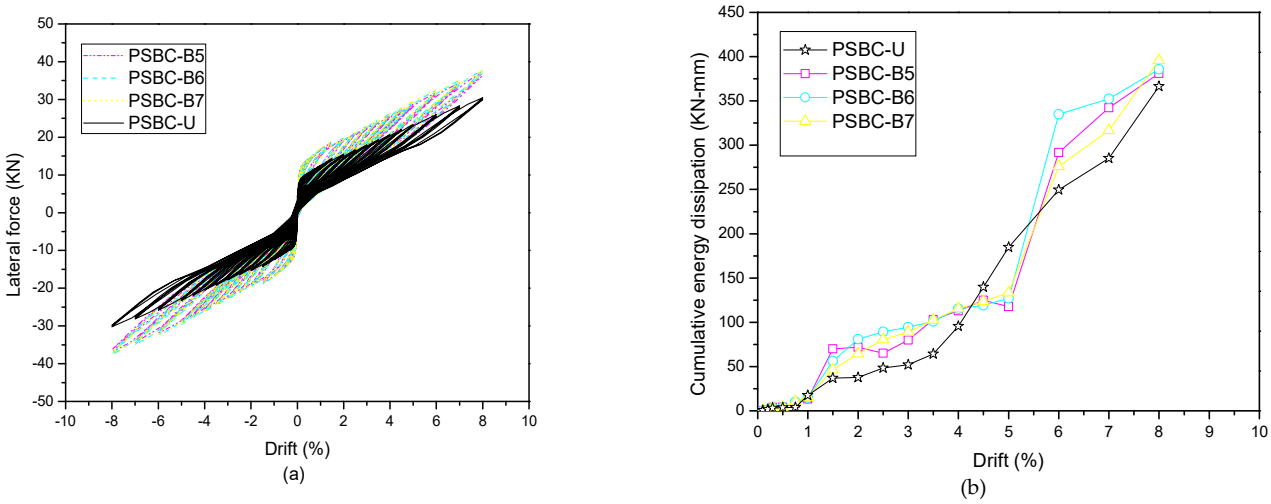

Figure 9. (**a**) Lateral force of hybrid-bonded and unbonded PSBCs in non-hinge area (**b**) Cumulative energy dissipation curves of hybrid-bonded and unbonded PSBCs in non-hinge area.

To achieve the ultimate lateral strength and energy dissipation, all three models bonded in the non-plastic hinge region performed similarly with slight changes in the maximum values. PSBC-B7 obtained the maximum strength with the highest value of 45.34 KN in the positive direction, which is 20.72% greater than PSBC-U. In contrast, for energy dissipation, PSBC-B7 could dissipate a maximum energy of 395.89 (KN-mm), which is 7.46% greater than PSBC-U. The residual drift values shown in Table 7 show a similar pattern, which leads to the conclusion that bonding tendons across non-plastic hinge regions are not as adequate as bonding across plastic hinge regions. The limit-state capacity analysis indicates a decrease in the displacement capacity, ductility, and limit-

state lateral strength along with similar initial elastic stiffness and yield lateral strength values, with an increase in the bonded length across the non-plastic hinge region, as shown in Table 7. It must be noted that the distance of the non-plastic hinge from the hinge zone was very high. Selecting segments near the plastic hinge area may lead to better results, which can be compared with plastic hinge region results in future analysis.

6.1.3. Hybrid Bonding across the Critical Joint

The usage of bonded tendons in the plastic hinge and non-plastic hinge region has been discussed in the previous sections. This section discusses the effect of bonded tendons across the bottom joint (joint between segment S-4 and footing). PSBC-B8 and PSBC-B9 had a 100 mm bonded length across the bottom joint and a 50% and 75% bonded length in the plastic hinge region, whereas PSBC-B10 and PSBC-B11 had a 50%, 75%, and 300 mm bonded length in the plastic hinge and across the bottom joint, respectively. The hysteric energy dissipation curves are shown in Figure 10a,b, and a comparison of various response parameters is shown in Table 8.

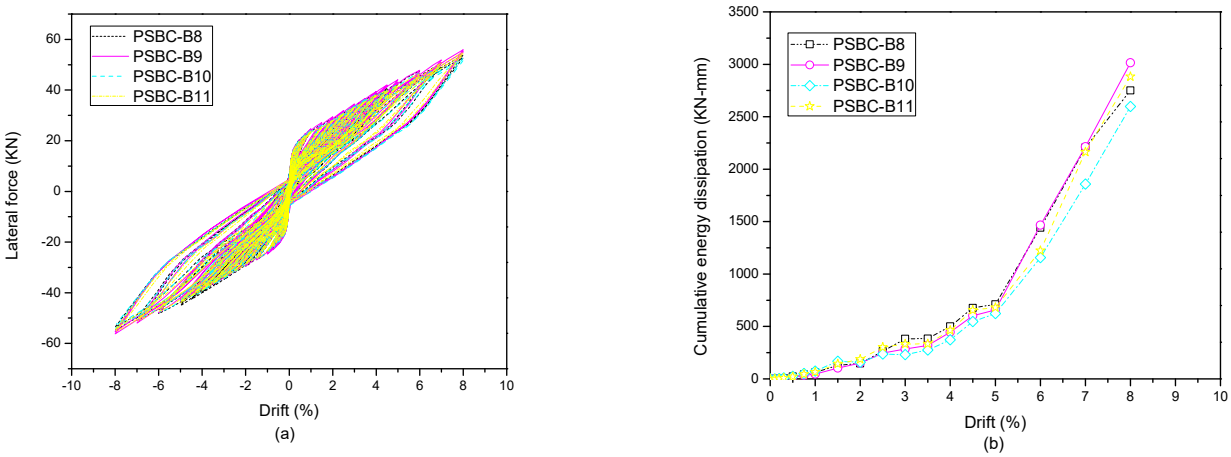

Figure 10. (**a**) Hysteric forces of PSBCs bonded in the plastic hinge and across the bottom joint. (**b**) Cumulative energy dissipation curves of PSBCs bonded in the plastic hinge and across the bottom joint.

Table 8. Comparison of the response parameters of PSBC models bonded across the critical joint with the ones bonded only in the plastic hinge region.

Specimen	Yield State		Limit State		Displacement Ductility Ratio	Residual Displacement (mm)	Ultimate Strength (KN)
	Force (KN)	Drift (%)	Force (KN)	Drift (%)			
PSBC-B8	29.28	1	33.84	3	3	11, −9.34	52.81, −53.56
PSBC-B9	26.6	1.389	34.52	3	2.15	14.67, −13.48	55.14, −55.37
PSBC-B10	24.23	1	36.29	3.23	3.23	9.8, −9.02	51.65, −52.86
PSBC-B11	22.35	1.21	35.89	3.15	2.603	13.65, −12.89	54.37, −54.78
PSBC-B12	32.27	2	39.15	3.16	1.58	52, −49.95	60.73, −61.09
PSBC-B2	23.83	1.5	37.72	5	3.33	8.86, −5.96	47.89, −48.23
PSBC-B3	24.45	1.6	38.6	4.5	2.812	9.01, −8.73	46.84, −48.05
PSBC-B4	29.52	2.5	39.01	4	1.6	37.38, −37.64	51.85, −51.73

PSBC-B9 had increased ultimate lateral strength and residual drift values compared to PSBC-B8, which lead to a 10% greater level of energy dissipated for the later model. More importantly, PSBC-B9 generated higher ultimate lateral strength (15.4%) and energy dissipation (48.19%) than PSBC-B3, which had the same bonded length in the plastic hinge

region. Compared with PSBC-B4, which had the highest energy dissipation capacities with residual drifts crossing 2%, PSBC-B9 generated increased lateral strength, capturing 75% of the energy dissipated, while keeping residual drifts under the safety limits of 1%. At the same time, PSBC-B3 was only able to capture 25% of the energy dissipated. As far as PSBC-B10 and PSBC-B11 are concerned, the reduced lateral strengths, energy dissipation, and residual drift values can be attributed to the selection of the bonded length across the joint; the increased bonded length across the joint leads to decreasing values.

The detailed analysis of the limit-state capacities shows that when the length across the footing is kept constant, increasing the bonded length in the plastic hinge region increases the yield drift, ultimate strength, and plastic deformation of piers. In contrast, there is a decrease in the displacement capacity, ductility, and yield-bearing capacity of piers. If the bonded length of tendons in the plastic hinge region is kept constant, increasing the bonded length in the bearing platform decreases the initial elastic stiffness, ultimate strength, and residual displacement while increasing the piers' displacement capacity, limit-state strength, and ductility.

The comparative analysis between the specimens bonded in the plastic hinge region to those bonded in the plastic hinge and the critical joint shows that the yield lateral strength improves by bonding tendons across the critical joint. However, its contribution decreases when the bonded length is increased from 100 mm to 300 mm, as shown in Table 8. In contrast, the limit-state lateral strength and the ductility decrease by bonding tendons across the bearing platform with a decreasing contribution when the bonded length increases from 100 mm to 300 mm, respectively. The initial elastic stiffness and displacement capacity of PSBCs bonded across the critical joint was lower than that of piers bonded only partially in the plastic hinge region.

Finally, PSBC-B12, which has a 100% bonded length in the plastic hinge region and 300mm across the bottom joint, is compared with PSBC-B4 (100% bonded across the plastic hinge region); its lateral force curves in Figure 11a and energy dissipation curves in Figure 11b show that bonding more than 75% in the plastic hinge along with a combination of bonding across the bottom joint will lead to a higher yield and ultimate lateral strength and energy dissipation. However, since the column attains higher residual drifts (>2.5%) along with decreasing initial elastic stiffness and displacement capacity, it may lead to column failure or reaching a non-repairable level.

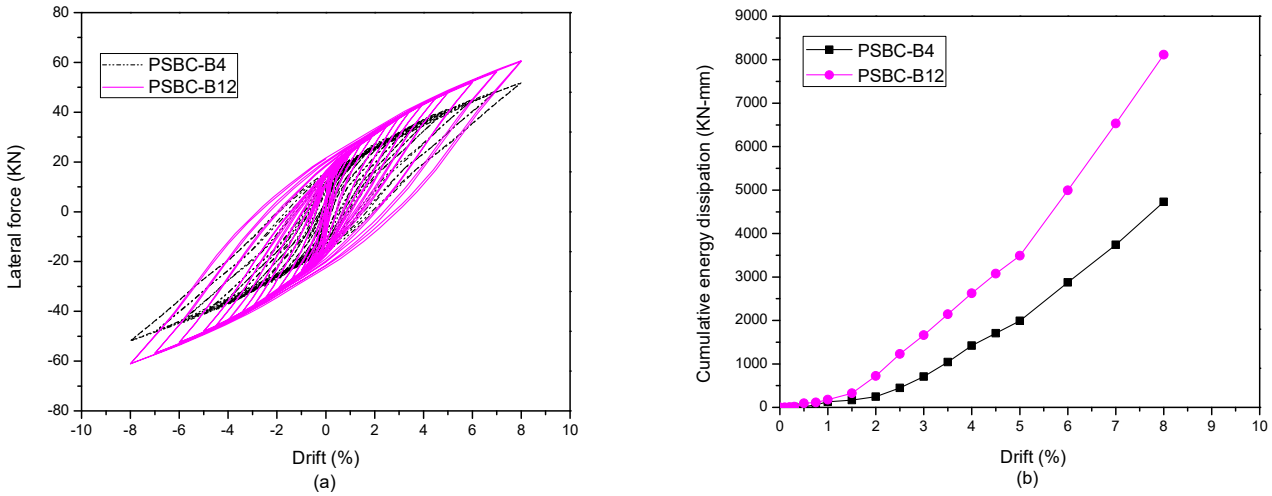

Figure 11. Comparison of hybrid-bonded PSBCs' (**a**) lateral force and (**b**) cumulative energy dissipation.

Overall, it may be concluded that the careful selection of the bonded length in the plastic hinge region and across the bottom joint can lead to improved lateral strength and

energy dissipation, as well as restraining residual displacement under safety limits after the application of cyclic loads. This novel concept offers a cost-effective and simpler design compared to existing methods, such as combinations of cast-in-place and segmental columns, steel jacketing, and elastomeric pads. It outperforms unbonded and bonded tendons in terms of lateral strength, energy dissipation, and lower residual drifts, making it a promising alternative for future study.

6.2. Energy Dissipation (ED) Bars

Using internal bars as the bonded mild reinforcement across the segment joints, also referred to as (ED bars), has proven to be an effective method to dissipate energy and control the elongation of the crack width. Pier's research focused on different designs and concepts of ED bars, such as bar ratios [38], equivalent plastic hinge modeling [53,54], and ED bars' contribution to the expected column strength [33]. This research focuses on the effect of different configurations (length and spreading) of ED bars on the overall seismic performance of PSBC.

Different Lengths of ED Bars

Here, 6D12 mm ED bars are added to the column, and specimens are denoted as PSBC-E1, PSBC-E2, PSBC-E3, and PSBC-E4, as detailed in Table 5. These bars start from the footing and extend to the middle and top of bottom segments 1 and 2, respectively, as shown in Figure 12. The ED bars are distributed evenly at a distance of 144 mm from the column center. ED bars are modeled with beam elements (B31); these bars are embedded in the surrounding concrete by using embedded constraints in a similar way to the longitudinal and transverse reinforcements, except for the equivalent (Leu) and additional unbounded length (Lau). Lau, 200 mm below the bottom segment, and Leu, 25 mm on both sides of the bottom segment joint, were selected for the model [34] to avoid the premature failure of the ED bars. In practice, PVC pipes or duct tape can cover the steel bars to separate them from the surrounding concrete. The elastic–perfectly plastic model was utilized for the ED bars, and the mechanical properties are shown in Table 9.

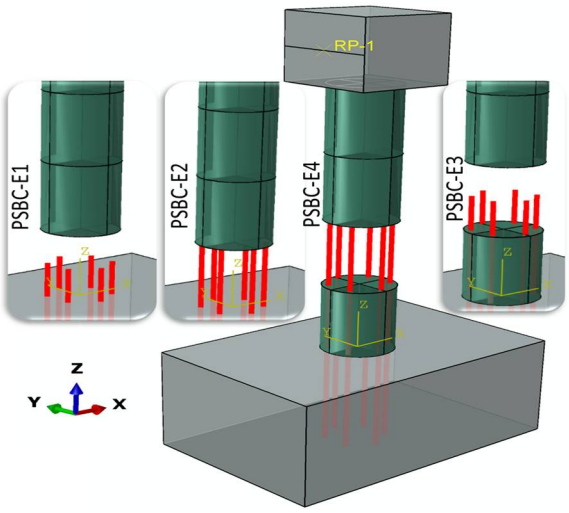

Figure 12. Graphical representation of ED bars with different lengths.

Table 9. Mechanical properties of ED bars.

Component	Property	Value
ED bars	Density (kg/m^3)	7800
	Yield stress (MPA)	335.0
	Poisson's ratio	0.3
	Elastic modulus (GPA)	200

The detailed hysteric and energy dissipation curves are shown in Figure 13a,b, and response parameters at the limit-state capacities and maximum drift ratio are shown in Table 10. Using ED bars helps increase the lateral strength and energy dissipation, respectively. A particular pattern develops, which can be stated as a) increasing the length of ED bars in the bottom segment leads to similar ultimate lateral strengths and energy dissipation capacities because increasing the length decreases the strain in the bars [52]. It is accurate if the column is made of one segment or the bars do not cross more than one joint, as is the case with PSBC-E1 and PSBC-E2. However, when the length of the ED bars crosses more than one segment joint, increasing the length leads to an increase in the ultimate lateral strength and residual drifts, which results in the increased overall energy dissipation of the system, as can be seen in PSBC-E3 and PSBC-E4, respectively.

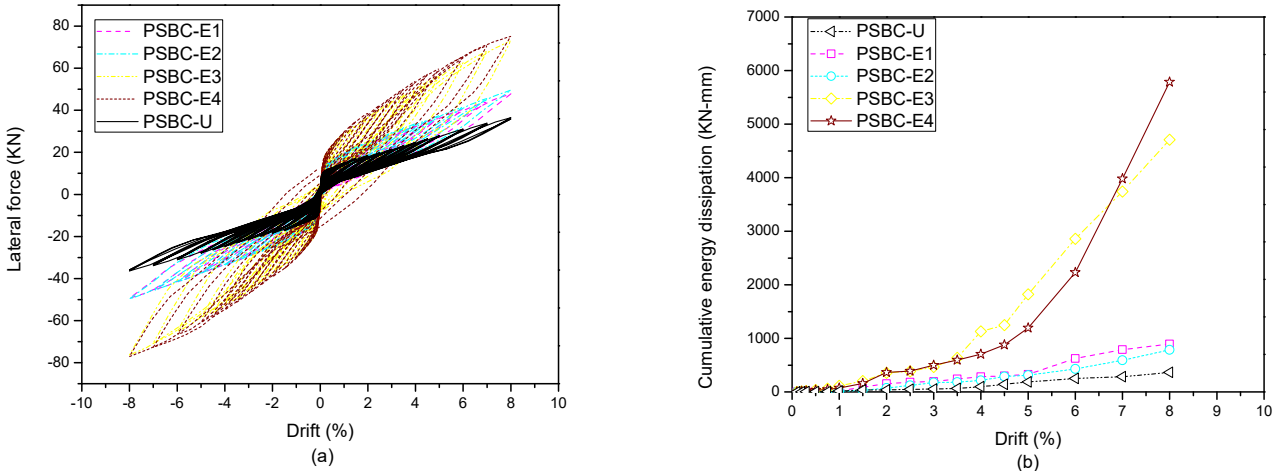

Figure 13. (**a**) Hysteric force of PSBCs with ED bars (**b**) Cumulative energy dissipation curves of PSBCs with ED bars.

Table 10. Response parameters of specimens with different lengths of ED bars.

Specimen	Yield State		Limit State		Displacement Ductility Ratio	Residual Displacement (mm)
	Force (KN)	Drift (%)	Force (KN)	Drift (%)		
PSBC-E1	21.03	1.36	36.67	5	3.67	7.22, −1.29
PSBC-E2	22.98	1.6	37.50	5	3.12	6.45, −1.15
PSBC-E3	28.30	0.94	44.29	3	3.19	17.27, −9
PSBC-E4	31.87	1.204	41.31	2.43	2.01	33.86, −25

The limit-state capacity analysis shows an increase in the length of ED bars, which improved both the initial elastic stiffness and the horizontal yield strength. In contrast, the ductility decreased when the ED bars crossed single and multiple precast joints. The limit-state bearing capacity increased when the ED bars crossed a single joint. In contrast, the limit-state bearing capacity decreased with an increase in the length of the ED bars crossing multiple joints. The displacement capacity remained the same when the ED bars crossed a single joint, but decreased with an increase in the length of ED bars crossing

multiple joints, as shown in Table 10. The overall residual drift of piers remained under 1% for all but PSBC-E4, which can be seen in Table 10, indicating that the length of the ED bars directly affects the recentering capabilities of piers. Hence, care must be taken while designing the length of ED bars. PSBC-E3 proved to be an excellent design length in this analysis, as it successfully provided an optimal performance. In the rare event of an earthquake force causing a potential fracture of the ED bars in PSBCs, the columns will still exhibit flag-shape hysteric behavior, characterized by high energy dissipation and minimal residual displacements. This behavior is maintained because well-designed prestressed tendons assist PSBCs in retaining their recentering abilities. The proper selection of other key factors such as axial load, concrete strength, reinforcing bars, and the ratio of ED bars further contributes to this resilience. In conclusion, even if ED bars fracture due to high loads, appropriately designed PSBC systems are unlikely to experience immediate collapse.

6.3. Orientation of ED Bars

The addition of ED bars was an effective measure to increase the system's bearing capacity and energy dissipation while maintaining its recentering abilities. This section presents a detailed parametric study focusing on the circumferential spreading of the ED bars with varying longitudinal lengths in the PSBC. The position of ED bars plays a vital role in the overall cyclic performance of PSBC as the behavior of ED bars changes with different distances from the column center. However, this fact has not been thoroughly studied for PSBCs so far. For this purpose, ED bars were added at a distance of 30%, 50%, 70%, and 90% of the core concrete circumference, as shown in Figure 14, and specimen details are shown in Table 5.

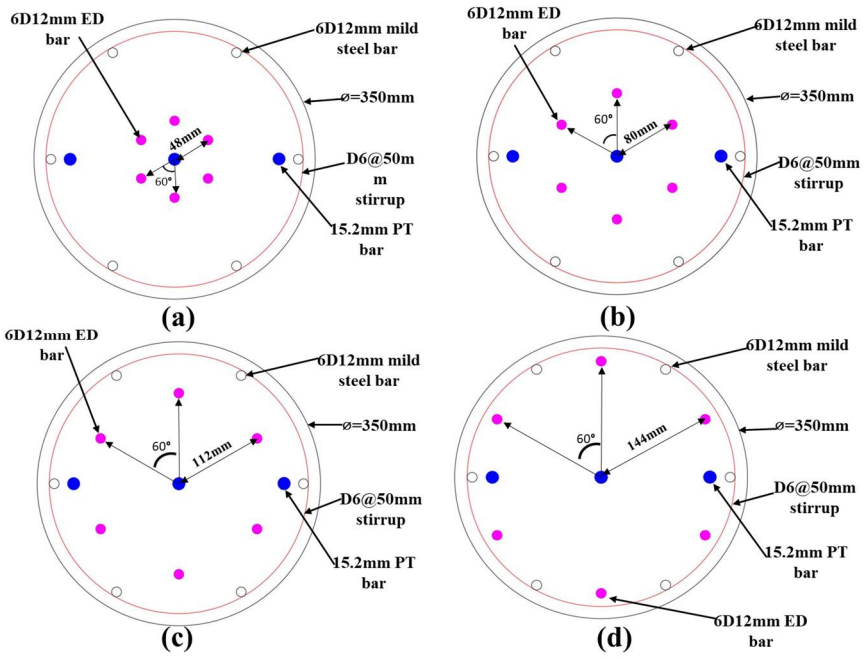

Figure 14. Different spreading of ED bars (**a**) PSBC-S30, (**b**) PSBC-S50, (**c**) PSBC-S70, and (**d**) PSBC-S90.

6.3.1. Orientation of ED Bars Crossing a Single Precast Joint

The length of the ED bars reached the middle and top of the bottom precast segment. Similar results were observed in terms of the ultimate lateral strength when the ED bars reached the middle and top of the bottom segment. The dissipated energy gradually de-

creased as the ED bars were oriented near the center for all but PSBC-S70E2, whose dissipated energy dropped by 23%. This drop is attributed to the residual plastic displacement, as shown in Table 11.

The limit-state capacity analysis showed similar results when the ED bars reached the middle of the bottom segment. In contrast, the initial elastic stiffness, displacement capacity, yield strength, and limit-state bearing capacity decreased when the ED bars were oriented near the center. In contrast, the ductility improved, as shown in Table 11.

Table 11. Response parameters of ED bars crossing a single precast joint.

Specimen	Yield State		Limit State		Displacement Ductility Ratio	Residual Displacement (mm)	Ultimate Strength (KN)	Dissipated Energy (KN-mm)
	Force (KN)	Drift (%)	Force (KN)	Drift (%)				
PSBC-S90E1	21.03	1.36	36.67	5	3.67	7.3, −9.25	47.8, −49.3	894.25
PSBC-S70E1	21.78	1.35	36.93	5	3.7	7.8, −9.15	48.4, −49.1	865.32
PSBC-S50E1	21.70	1.35	36.96	5	3.7	10.2, −13.25	47.5, −48	860.82
PSBC-S30E1	21.81	1.36	36.86	5	3.67	8.4, −9.25	47.7, −48.7	861.81
PSBC-S90E2	22.98	1.6	37.50	5	3.125	6.45, −8.5	49.56, −49.7	805.96
PSBC-S70E2	20.13	1.206	34.64	4.5	3.73	3.87, −1.28	48.48, −49.16	654.9
PSBC-S50E2	20.75	1.217	35.06	4.5	3.69	8.55, −11.34	47.52, −48.09	787.3
PSBC-S30E2	21.81	1.39	35.62	4.5	3.23	6.25, −10.55	47.71, −48.71	774.75

6.3.2. Orientation of ED Bars Crossing Multiple Precast Joints

The ED bars crossed multiple precast joints, and there was a significant change in the cyclic performance of specimens with different spreads at these levels of the ED bars' length. The ultimate lateral strength curves are shown in Figure 15a,b. The peak strengths were observed when the ED bars were oriented near the edges of the specimens, as shown in Table 12.

Table 12. Response parameters of ED bars crossing multiple precast joints.

Specimen	Yield State		Limit State		Displacement Ductility Ratio	Residual Displacement (mm)	Ultimate Strength (KN)	Dissipated Energy (KN-mm)
	Force (KN)	Drift (%)	Force (KN)	Drift (%)				
PSBC-S90E3	28.30	0.94	44.29	3	3.19	17.87, −9.14	73.12, −77.11	4707.65
PSBC-S70E3	27.90	0.92	44	3.17	3.42	30.6, −28.8	68.31, −69.81	5766.86
PSBC-S50E3	28.57	1.06	43.80	3.16	2.98	36, −34.2	58.23, −57.55	5050.62
PSBC-S30E3	28.34	1.05	44.14	3.16	3.009	38.5, −34.2	54.25, −54.18	3917.25
PSBC-S90E4	31.87	1.20	41.31	2.43	2.01	33.86, −25	75.25, −77.11	5786.38
PSBC-S70E4	30.45	1.15	41	2.22	1.93	40, −36.6	68.31, −69.81	6712
PSBC-S50E4	28.77	1.06	35.47	2	1.88	50.45, −54	58.23, −57.55	5850.49
PSBC-S30E4	29.72	1.20	35.99	2	1.66	38.88, −39	54.25, −54.18	3960.56

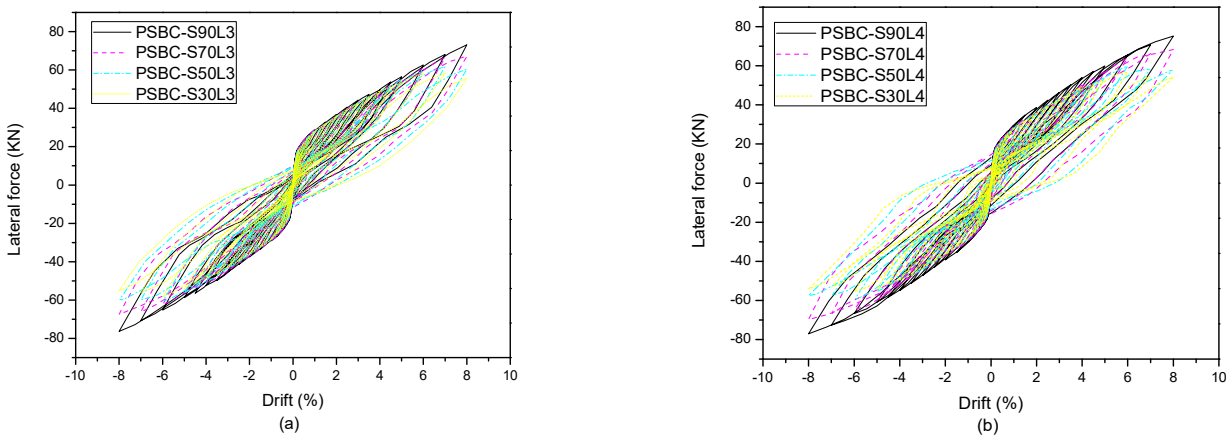

Figure 15. (**a**) Ultimate lateral strengths of ED bars' multiple precast joints with length L3 (**b**) Ultimate lateral strengths of ED bars' multiple precast joints with length L3.

Strength reduction was observed at 6% drift for the specimens whose ED bars were spread near the center, and its contribution increased with the decreasing values of circumferential spread. The specimens oriented at a distance of 70% of the core concrete circumference were able to dissipate maximum energy with a peak increase of 47–76% when compared to specimens spread at 30%. There was a slight improvement in the dissipated energy for the ED bars oriented at 50% spread to the ones oriented at 90% spread. However, due to the latter model's better ultimate bearing capacity, reduced residual plastic deformation, and the former strength reduction, PSBC-S90L3, and PSBC-S90L4 are better candidates for the seismic regions. Furthermore, the displacement capacity, ductility, and limit-state bearing capacities of ED bars oriented near the edges were more significant than those of ED bars oriented near the center, as shown in Table 12. Finally, for all the spreads, it was observed that energy dissipation and residual drift increase with an increase in length when the ED bars cross multiple joints, whereas the residual drift increases and the energy dissipation decreases when ED bars cross a single joint

The primary reason for applying ED bars is to improve the energy dissipation of PSBC. The drop in ductility is apparent, but it must be kept within reasonable levels. Hence, in this analysis, it is observed that the spread of ED bars near the edges of the section leads to satisfactory ductility and an overall superior cyclic performance.

Energy dissipation (ED) bars provide superior energy dissipation and lateral strength while minimizing residual displacement, offering a cost-effective and straightforward solution for enhancing the seismic performance of bridge columns compared to alternatives like elastomeric pads, steel shear-resistant connectors, and hybrid steel bars. The detailed limit-state analysis further emphasizes this key advantage.

7. Conclusions

This paper investigated the cyclic performance of PSBCs, focusing on ways to improve the lateral strength energy dissipation and reduce the residual deformation. The influence of hybrid-bonded tendons was analyzed by studying the hysteric curves of PSBCs. Afterward, a thorough study was presented, which detailed the effects of the addition of ED bars to the PSBCs. Different longitudinal lengths and circumferential spreads of ED bars crossing the precast joints were chosen to improve the hysteric characteristics of PSBCs. The key findings are listed as follows:

- Hybrid bonding in the plastic hinge region improves the lateral strength, energy dissipation, initial elastic stiffness, and horizontal yield-bearing capacity of PSBCs compared to PSBCs with unbonded post-tensioned tendons.

- At higher lateral loads, hybrid bonding completely across the plastic hinge region showed a better ultimate bearing capacity and energy dissipation. However, the attainment of residual displacements greater than the 1% safety limit and a decreased ductility and displacement capacity makes a bonded tendon length of 25–75% in the plastic hinge region a better option to prevent column failure.
- Hybrid bonding at 75% in the plastic hinge region and 100 mm–300 mm in footing is suitable for medium–high seismic regions because of the improved lateral strength, minimal residual deformations, and adequate energy dissipation and tensile capacity.
- The addition of ED bars in PSBCs crossing two precast segment joints showed a significant increase in the lateral strength energy dissipation while maintaining the recentering abilities, compared to PSBCs with the ED bars crossing the single joint.
- The circumferential spread of 70–90% along the core concrete is a better option due to the strength degradation and significant surge in residual deformations observed in the 30–50% spread of ED bars.

Author Contributions:. Conceptualization, J.B. and M.A.; methodology, J.B.; software, J.B.; validation, J.B. and M.A.; formal analysis, J.B. and M.A.; investigation, J.B.; resources, T.U.; data curation, N.A.; writing—original draft preparation, J.B. and M.A.; writing—review and editing, Q.S., N.A. and M.U.A.; visualization, M.U.A.; supervision, W.C.; project administration, T.U. and W.C.; funding acquisition, T.U. All authors have read and agreed to the published version of the manuscript

Funding:. This work was supported by Supported by the Science and Technology Research Program of the Institute of Mountain Hazards and Environment, CAS (IMHE-ZDRW-01), and the National Natural Science Foundation of China, China (Grant numbers: 42077275 & 42271086), and the Special project of Basic Research-Key project, Yunnan (Grant numbers: 202301AS070039).

Data Availability Statement: The datasets generated during and/or analyzed during the current study are available from the corresponding author upon reasonable request.

Conflicts of Interest:. Authors declare there is no conflict of interest.

References

1. Ou, J.P.; Li, H. The regional engineering damage and reconstruction strategy in Wenchuan earthquake of China. *J. Earthq. Tsunami* **2011**, *5*, 189–216.
2. Wang, Z.; Ge, J.; Wei, H.; Liu, F. Recent development in seismic research of segmental bridge columns. *J. Earthq. Eng. Eng. Vib.* **2009**, *4*, 147–154.
3. Hongnan, L.; Linsheng, H. Recent developments of structural vibration control in civil engineering in China. *J. Earthq. Tsunami* **2010**, *4*, 9–21.
4. Wacker, J.M.; Hieber, D.G.; Stanton, J.F.; Eberhard, M.O. *Design of Precast Concrete Piers for Rapid Bridge Construction in Seismic Regions (No. WA-RD 629.1)*; University of Washington: Seattle, WA, USA, 2005.
5. Hällmark, R.; White, H.; Collin, P. Prefabricated bridge construction across Europe and America. *Pract. Period. Struct. Des. Constr.* **2012**, *17*, 82–92.
6. Liu, X.; Li, J.; Tsang, H.H.; Wilson, J.L. Evaluating self-centering behavior of unbonded prestressed bridge columns using a new performance index based on quasi-static analysis. *J. Earthq. Tsunami* **2018**, *12*, 1850001.
7. Motaref, S.; Saiidi, M.S.; Sanders, D. Shake table studies of energy dissipating segmental bridge columns. *J. Bridge Eng.* **2013**, *19*, 186–199.
8. Billington, S.L.; Yoon, J.K. Cyclic response of unbonded posttensioned precast columns with ductile fiber reinforced concrete. *J. Bridge Eng.* **2004**, *9*, 353–363.
9. ElGawady, M.A.; Sha'lan, A. Seismic behavior of self-centering precast segmental bridge bents. *J. Bridge Eng.* **2010**, *16*, 328–339.
10. Mohebbi, A.; Saiidi, M.S.; Itani, A.M. Shake table studies and analysis of a precast two column bent with advanced materials and pocket connections. *J. Bridge Eng.* **2018**, *23*, 04018046.
11. Zhang, Y.; Fan, W.; Zhai, Y.; Yuan, W. Experimental and numerical investigations on seismic behavior of prefabri-cated bridge columns with UHPFRC bottom segments. *J. Bridge Eng.* **2019**, *24*, 04019076.
12. ElGawady, M.; Booker, A.J.; Dawood, H.M. Seismic behavior of posttensioned concrete filled fiber tubes. *J. Compos. Constr.* **2010**, *14*, 616–628.
13. Mander, J.B.; Cheng, C.T. *Seismic Resistance of Bridge Piers Based on Damage Avoidance Design*; University at Buffalo: Amherst, NY, USA, 1997.

14. Hewes, J.T.; Priestley, M.N. *Seismic Design and Performance of Precast Concrete Segmental Bridge Columns (No. SSRP-2001/25*); University of California: San Diego, CA, USA, 2002.
15. J Chou, C.C.; Chen, Y.C. Cyclic tests of post tensioned precast CFT segmental bridge columns with unbonded strands. *Earthq. Eng. Struct. Dyn.* **2006**, *35*, 159–175.
16. Ou, Y.C.; Oktavianus, Y.; Tsai, M.S. An emulative precast segmental concrete bridge column for seismic regions. *Earthq. Spectra* **2013**, *29*, 1441–1457.
17. Kim, D.H.; Kim, M.K.; Zi, G.; Roh, H. Experimental test and seismic performance of partial precast concrete seg-mental bridge column with cast in place base. *Eng. Struct.* **2015**, *100*, 178–188.32.
18. Zhang, Y.; Wu, G.; Dias-da-Costa, D. Cyclic loading tests and analyses of posttensioned concrete bridge columns combining cast in place and precast segments. *Bull. Earthq. Eng.* **2019**, *17*, 6141–6163
19. Jia, J.; Zhang, K.; Saiidi, M.S.; Guo, Y.; Wu, S.; Bi, K.; Du, X. Seismic evaluation of precast bridge columns with built in elastomeric pads. *Soil Dyn. Earthq. Eng.* **2020**, *128*, 105868.
20. Kim, T.H.; Lee, H.M.; Kim, Y.J.; Shin, H.M. Performance assessment of precast concrete segmental bridge columns with a shear resistant connecting structure. *Eng. Struct.* **2010**, *32*, 1292–1303.
21. Mao, J.; Jia, D.; Yang, Z.; Xiang, N. Seismic Performance of Concrete Bridge Piers Reinforced with Hybrid Shape Memory Alloy (SMA) and Steel Bars. *J. Earthq. Tsunami* **2019**, *14*, 2050001
22. Yamashita, R.; Sanders, D.H. Seismic performance of precast unbonded prestressed concrete columns. *ACI Struct. J.* **2009**, *106*, 821–830.
23. Ou, Y.C.; Wang, P.H.; Tsai, M.S.; Chang, K.C.; Lee, G.C. Large scale experimental study of precast segmental unbonded post-tensioned concrete bridge columns for seismic regions. *J. Struct. Eng.* **2009**, *136*, 255–264.
24. Bu, Z.Y.; Ding, Y.; Chen, J.; Li, Y.S. Investigation of the seismic performance of precast segmental tall bridge columns. *Struct. Eng. Mech.* **2012**, *43*, 287–309.
25. Nikbakht, E.; Rashid, K.; Hejazi, F.; Osman, S.A. A numerical study on seismic response of self-centering precast segmental columns at different post tensioning forces. *Lat. Am. J. Solids Struct.* **2014**, *11*, 864–883.
26. Shim, C.; Lee, S.; Park, S.; Koem, C. Experiments on prefabricated segmental bridge piers with continuous longitudinal rein-forcing bars. *Eng. Struct.* **2017**, *132*, 671–683.
27. Wang, Z.; Song, W.; Wang, Y.; Wei, H. Numerical analytical model for seismic behavior of prestressing concrete bridge column systems. *Procedia Eng.* **2011**, *14*, 2333–2340.
28. Wang, Z.; Ge, J.; Wei, H. Seismic performance of precast hollow bridge piers with different construction details. *Front. Struct. Civ. Eng.* **2014**, *8*, 399–413.
29. Marriott, D.; Pampanin, S.; Palermo, A. Quasi static and pseudo dynamic testing of unbonded post tensioned rocking bridge piers with external replaceable dissipaters. *Earthq. Eng. Struct. Dyn.* **2009**, *38*, 331–354.
30. Kam, W.Y.; Pampanin, S.; Palermo, A.; Carr, A.J. Self-centering structural systems with combination of hysteretic and viscous energy dissipations. *Earthq. Eng. Struct. Dyn.* **2010**, *39*, 1083–1108.
31. Guo, T.; Cao, Z.; Xu, Z.; Lu, S. Cyclic load tests on self-centering concrete pier with external dissipators and enhanced durability. *J. Struct. Eng.* **2015**, *142*, 04015088.
32. Palermo, A.; Pampanin, S.; Marriott, D. Design, modeling, and experimental response of seismic resistant bridge piers with posttensioned dissipating connections. *J. Struct. Eng.* **2007**, *133*, 1648–1661
33. Ou, Y.C.; Tsai, M.S.; Chang, K.C.; Lee, G.C. Cyclic behavior of precast segmental concrete bridge columns with high performance or conventional steel reinforcing bars as energy dissipation bars. *Earthq. Eng. Struct. Dyn.* **2010**, *39*, 1181–1198.
34. Bu, Z.Y.; Ou, Y.C.; Song, J.W.; Zhang, N.S.; Lee, G.C. Cyclic loading test of unbonded and bonded posttensioned precast segmental bridge columns with circular section. *J. Bridge Eng.* **2015**, *21*, 04015043.
35. Moon, D.Y.; Roh, H.; Cimellaro, G.P. Seismic performance of segmental rocking columns connected with NiTi martensitic SMA bars. *Adv. Struct. Eng.* **2015**, *18*, 571–584.
36. Cai, Z.K.; Wang, Z.; Yang, T.Y. Experimental testing and modeling of precast segmental bridge columns with hybrid normal and high strength steel rebars. *Constr. Build. Mater.* **2018**, *166*, 945–955.
37. Wang, J.C.; Ou, Y.C.; Chang, K.C.; Lee, G.C. Large-scale seismic tests of tall concrete bridge columns with precast segmental construction. *Earthq. Eng. Struct. Dyn.* **2008**, *37*, 1449–1465.
38. Li, C.; Hao, H.; Bi, K. Numerical study on the seismic performance of precast segmental concrete columns under cyclic loading. *Eng. Struct.* **2017**, *148*, 373–386.
39. Wang, J.; Wang, Z.; Tang, Y.; Liu, T.; Zhang, J. Cyclic loading test of self-centering precast segmental unbonded posttensioned UHPFRC bridge columns. *Bull. Earthq. Eng.* **2018**, *16*, 5227–5255.
40. Zhang, X.; Xu, S.; Zhang, S.; Xu, G. Experimental Investigations on the Seismic Behavior of Precast Concrete Columns with Novel Box Connections. *J. Earthq. Tsunami* **2019**, *14*, 2050007.
41. Ministry of Transport of the People's Republic of China—MOT. *Guidelines for Seismic Design of Highway Bridges (JTG/T B02-01-2008)*; Ministry of Transport of the People's Republic of China: Beijing, China, 2008. (In Chinese)
42. Nielson, B.G.; Desroches, R. Analytical seismic fragility curves for typical bridges in the central and southeastern United States. *Earthq. Spectra* **2012**, *23*, 615–633.
43. Zhang, Y.; Dias-da-Costa, D. Seismic vulnerability of multi-span continuous girder bridges with steel fibre rein-forced concrete columns. *Eng. Struct.* **2017**, *150*, 451–464.

44. Japan Road Association. *Design Specification of Highway Bridge: Part V-Seismic Design (JRA 2002)*; Japan Road Association: Tokyo, Japan, 2002. (In Japanese)
45. Wang, Z.; Wang, J.Q.; Zhu, J.Z. Pushover analysis of precast segmental UHPFRC bridge columns with unbonded posttensioned tendons. *Key Eng. Mater.* **2018**, *765*, 391–396.
46. Nikbakht, E. Seismic Behaviour of Post-Tensioned Segmental Bridge Columns with Self-Centring System. In *Earthquakes-Tectonics, Hazard and Risk Mitigation*; IntechOpen: London, UK, 2017.
47. SIMULIA. *ABAQUS 6.14 Commercial Computer Software Documentation*; SIMULIA: Providence, RI, USA, 2012.
48. Wang, Z.; Wang, J.; Tang, Y.; Gao, Y.; Zhang, J. Lateral behavior of precast segmental UHPC bridge columns based on the equivalent plastic hinge model. *J. Bridge Eng.* **2018**, *24*, 04018124.
49. Lubliner, J.; Oliver, J.; Oller, S.; Oñate, E. A plastic damage model for concrete. *Int. J. Solids Struct.* **1989**, *25*, 299–326.
50. Lee, J.; Fenves, G.L. Plastic damage model for cyclic loading of concrete structures. *J. Eng. Mech.* **1998**, *124*, 892–900.
51. Chen, W.R.; Wang, T.C.; Yan, D. *Concrete Structure: Design Principle of Concrete Structure*; Elsevier: Amsterdam, The Netherlands, 2012.
52. Dawood, H.; ElGawady, M.; Hewes, J. Behavior of segmental precast posttensioned bridge piers under lateral loads. *J. Bridge Eng.* **2011**, *17*, 735–746.
53. Wang, Z.; Wang, J.; Zhu, J.; Zhao, G.; Zhang, J. Energy dissipation and self-centering capacities of posttensioning precast segmental ultra-high performance concrete bridge columns. *Struct. Concr.* **2019**, *21*, 517–532.
54. Leitner, E.J.; Hao, H. Three dimensional finite element modelling of rocking bridge piers under cyclic loading and exploration of options for increased energy dissipation. *Eng. Struct.* **2016**, *118*, 74–88.